DRAFT VERSION NOVEMBER 16, 2018
Typeset using LaTeX default style in AASTeX62

GD-1: the relic of an old metal-poor globular cluster

GUANG-WEI LI,[1] BRIAN YANNY,[2] AND YUE WU[3]

[1] *Key Laboratory for Optical Astronomy, National Astronomical Observatories, Chinese Academy of Sciences, Beijing 100101, China*
[2] *Fermi National Accelerator Laboratory, Batavia, IL 60510, USA*
[3] *National Astronomical Observatories, Chinese Academy of Sciences, Beijing 100101, China*

ABSTRACT

Combining data from Gaia DR2, SDSS DR14 and LAMOST DR6, we update the fit to model of the properties of the stellar stream GD-1 and find that it has an age of ~ 13 Gyr, [Fe/H] of -2.2 ± 0.12, and a distance from the sun of ~ 8 kpc. We tabulate 6D phase-space fiducial points along the GD-1 stream orbit over a $90°$ arc. The fitted orbit shows that the stream has an eccentricity $e \sim 0.3$, perigalacticon of 14.2 kpc, apogalacticon of 27.0 kpc and inclination $i \sim 40°$. There is evidence along the arc for 4 candidate stellar overdensities, one candidate gap, two candidate stellar underdensities and is cut off at $\phi_1 \sim 2°$ (in the stream-aligned (ϕ_1, ϕ_2) coordinate system of Koposov et al. (2010)). The spur originating at $\phi_1 \sim -40°$ implies stars were pulled away from the stream trace by an encounter (potentially a dark matter subhalo). The narrowest place (FWHM ~ 44.6 pc) of the GD-1 trace is at $(\phi_1, \phi_2^c) \sim (-14°, 0.15°)$, which is $\sim (178.18°, 52.19°)$ in (R. A., Decl.), where the progenitor is possibly located. We also find six BHB and 10 BS spectroscopic stars in the GD-1 stream.

Keywords: (Galaxy:) globular clusters: general — Galaxy: abundances — Galaxy: kinematics and dynamics — Galaxy: structure

1. INTRODUCTION

The stellar stream GD-1 was discovered by Grillmair & Dionatos (2006). It was traced over $63°$ on the sky (and now is known to extend over $\sim 90°$) but is only $\sim 0.5°$ wide. Using velocity and metallicity measures of stream members from the Sloan Extension for Galactic Understanding and Exploration (SEGUE) survey (Yanny et al. 2009), Willett et al. (2009) fit a retrograde orbit of perigalacticon 14.4 kpc, apogalacticon 28.7 kpc, inclination $i \sim 35°$ and [Fe/H] $= -2.1\pm0.1$. Later, Koposov et al. (2010) fit a 6D phase space map of the stream, which strongly constrains the circular velocity at the Sun's radius and the shape of the Galactic potential (also see Bowden et al. (2015); Bovy et al. (2016)). Koposov et al. (2010) also noted stellar density fluctuations along the stream, and conjectured that the clumps and holes may be related to either the history of the disruption process or interaction of the stream stars with dark matter subhalos around the Milk Way. Carlberg & Grillmair (2013) and Carlberg (2016) interpreted these gaps as massive dark matter subhalo encounters with this cold stellar stream. Recently, Price-Whelan & Bonaca (2018) find two big gaps and one spur along the GD-1 trace. The gap at $\phi_1 \sim -45°$ is also reported by de Boer et al. (2018). We also notice the work of Huang et al. (2018), but our work is different from it in both methods and contents.

In this paper, we refine GD-1 stream parameters and discuss all the topics mentioned above by combining data from Gaia DR2, SDSS DR14 and LAMOST DR6. This paper is organized as following: In Section 2, we will present the color-magnitude diagram(CMD), metallicity, 6D phase-space along the trace; Then the orbit fitting is practiced in Section 3; The stellar density fluctuation along the stream trace and blue horizontal branch(BHB) stars, and blue stragglers(BS) are discussed in Section 4; Finally, conclusions are given in Section 5.

lgw@bao.ac.cn

2. DATA

The data from Gaia DR2(Gaia Collaboration et al. 2018; Lindegren et al. 2018) and SDSS DR9 are crossed match using the database *gaiadr2.sdssdr9_best_neighbour* in TopCat (Taylor 2005). Parameters (T_{eff}, $\log g$, [Fe/H] and radial velocity (RV)) of the spectra from LAMOST DR6[1] (Cui et al. 2012; Zhao et al. 2012) are calculated by LASP (LAMOST Stellar Parameter Pipeline)(Wu et al. 2011a, 2014), and the main algorithm used in LASP is ULySS[2] (Koleva et al. 2008, 2009) with ELODIE interpolator(Wu et al. 2011b). We also use ULYSS with ELODIE interpolator to recalculate parameters of the spectra from SDSS DR14, so all spectral parameters used in this paper are all from the same pipeline. In the following, magnitudes with subscript 0 indicate they have been corrected by the extinction given by Schlafly & Finkbeiner (2011), which is 0.86 times those given by Schlegel et al. (1998), and we also denote $gr_0 \equiv g_0 - r_0$. We adopt in this paper the stream-centered (ϕ_1, ϕ_2) coordinate system and conversion equations given by Koposov et al. (2010). There are several papers in the literature which document a systematic underestimate of Gaia DR2 parallaxes, with varying shifts from -0.029 to -0.07 to -0.08 mas (Lindegren et al. 2018; Zinn et al. 2018; Stassun & Torres 2018). In this paper we adjust Gaia DR2 parallaxes by adding by 0.029 mas.

2.1. Astrometric and Photometric Data

Fig. 1 shows the proper motions of stars in the Gaia DR2 sample within $-60° < \phi_1 < -20°$ and $-0.2° < \phi_2 < 0.2°$. The overdensity at the bottom left corner clearly stands out. We select the GD-1 candidates with proper motions in the red polygon in Fig 1. Their CMDs from SDSS DR9 and Gaia DR2 are shown in the left and right panels of Fig. 2 respectively. Overlaid in the left panel, the red line is the best fit isochrone from the Dartmouth isochrone library(Dotter et al. 2008) with [Fe/H] = −2.3, an age of 13 Gyr, and a distance of 8 kpc. The area enclosed by the blue lines in Fig. 2 is

$$\begin{cases} gr_0 > -36.755917 + 6.1373654 \times g_0 - 0.34166210 \times g_0^2 + 0.0063657131 \times g_0^3 \\ gr_0 < 26.910462 - 3.9900350 \times g_0 + 0.19378849 \times g_0^2 - 0.0030286203 \times g_0^3 \\ 18.3 < g_0 < 21 \end{cases} \qquad (1)$$

Stars in this area are dwarfs, whose parallax distribution is shown in Fig. 3, where we can also see that almost all stars have $|\varpi| < 1$ mas. The red line is the fitting Gaussian function with a mean of 0.071 mas and a variance of 0.48 mas. Because of the big uncertainty, we cannot estimate the distance of GD-1 stream from the distribution. If we apply the parallax correction recommended in Stassun & Torres (2018), which is ~ -0.08 mas, we obtain an estimated typical distance to the stream center from the sun of ~ 8kpc.

We use the CMD of these dwarfs with $|\varpi| < 1$ mas and $-5° < \phi_2 < 1°$ to select GD-1 member candidates with distances in 8-10 kpc. We divide the full range where GD-1 candidate stars are detected $\phi_1 : [-85°, 5°]$ into 18 regions each with a 5° interval. Their diagrams of $\mu_\alpha cos\delta - \mu_\delta$ are shown in Fig. 4. The red circle in each panel is where we select GD-1 candidates. The radius of each circle is 2 mas/yr, which is large enough to cover most GD-1 members, while their fiducial centers are given in Table 1.

We select the overdensities in Fig. 4 by hand, then convert the circle centers in Fig. 4 to ($\mu_{\phi_1}, \mu_{\phi_2}$) coordinates. We also use the correction formula in Koposov et al. (2010) to correct the Sun's reflex motion (note that there is a typo in $\mu_{\phi_{1,2,c}} = \mu_{\alpha,\delta} - \mu_{reflex}$, which should be $\mu_{\phi_{1,2,c}} = \mu_{\alpha,\delta} + \mu_{reflex}$) by assuming the distance along ϕ_1: $d(\phi_1) = 8$ kpc if $\phi_1 < -20°$, $(\phi_1 + 20) \times 0.1$ kpc, otherwise, and $V_\odot = 220$ km/s. Fig. 5 shows the circle centers in Fig. 4 in (ϕ_1, μ) coordinate. In each panel, asterisks are μ_{ϕ_1}s, while diamonds are μ_{ϕ_2}s, and these circle centers are shown in red, while the data from Table 4 in Koposov et al. (2010) are shown in blue. The proper motions μ_{ϕ_1} and μ_{ϕ_2} in the right panel have been corrected for the Sun's reflex motion, while those in the left panel are not corrected. The left panel shows that these circle centers coincide well with data from Table 4 in Koposov et al. (2010), while the right panel shows that $\mu_{\phi_2} \sim 0$ mas/yr, which implies that GD-1 stars move along the GD-1 trace.

Fig. 6 and 7 show the $\mu_\alpha cos\delta$ and μ_δ of the stars in the circles in Fig. 4 along ϕ_1, respectively. We fit these $\mu_\alpha cos\delta$ and μ_δ by polynomials with the lowest orders that visually go right through the centers of these data along ϕ_1 in Fig. 6 and 7 respectively. The result polynomials are:

$$f_1(\phi_1) = -7.482 + 6.392 \times 10^{-2} \times \phi_1 + 4.553 \times 10^{-3} \times \phi_1^2 + 5.167 \times 10^{-5} \times \phi_1^3 + 1.950 \times 10^{-7} \times \phi_1^4 \qquad (2)$$

---

[1] http://dr6.lamost.org
[2] http://ulyss.univ-lyon1.fr

and

$$f_2(\phi_1) = -3.698 + 2.450 \times 10^{-1} \times \phi_1 - 5.795 \times 10^{-3} \times \phi_1^2 - 2.550 \times 10^{-4} \times \phi_1^3 - 2.858 \times 10^{-6} \times \phi_1^4 - 1.121 \times 10^{-8} \times \phi_1^5 \quad (3)$$

respectively. The red central line in Fig. 6 is $f_1(\phi_1)$, while that in Fig. 7 is $f_2(\phi_1)$. These two equations can correct small deviations of the circle centers in Fig. 4 selected by hand.

Now, we map the GD-1 stream using stars by the criteria: (1) They should be in the GD-1 dwarf CMD of 8-10kpc, (2) $|\varpi| < 1$ mas, and (3) They should be covered by the circles in Fig. 4. Fig. 8 shows positions of these stars, where the GD-1 overdensity clearly stands out and follows the trace. We select some fiducial points along the GD-1 trace in (ϕ_1, ϕ_2), which is listed in Table 2, then fit them by a quadratic polynomial:

$$f_3(\phi_1) = -1.057 - 7.030 \times 10^{-2} \times \phi_1 - 1.033 \times 10^{-3} \times \phi_1^2 \quad (4)$$

, which is the red line in Fig. 8. We also introduce

$$\phi_2^c(\phi_1) \equiv \phi_2 - f_3(\phi_1) \quad (5)$$

to help us further study the GD-1 stream.

To determine the distances of different parts of the GD-1 stream, we select stars by the criteria: (1) $|\varpi| < 1$ mas, (2) $|\phi_2^c| < 0.5°$, (3) $|\mu_\alpha cos\delta - f_2(\phi_1)| < 1$ mas/yr and (4) $|\mu_\delta - f_3(\phi_1)| < 1$ mas/yr. **The matched filter algorithm in Willett et al. (2009) is used to estimate the distances. We find that the stars of the GD-1 stream in Fig. 2 within $17 < g_0 < 21$ can be well bounded by $|gr_0(g_0) - \mathrm{ISO}(g_0)| < -0.312 + 0.019 \times g_0$ ($\mathrm{ISO}(g_0)$ is the Dartmouth isochrone with $[\mathbf{Fe/H}] = -2.3$, an age of 13 Gyr and a distance of 8 kpc), which is shown in Fig. 9, where the bound lines are shown in blue, stars are shown by black symbols and the red line is the Dartmouth isochrone with $[\mathbf{Fe/H}]= -2.3$, an age of 13 Gyr and a distance of 8 kpc. Thus we use $\sigma(g_0) = 0.5 \times (-0.312 + 0.019 \times g_0)$ for Gaussian profiles to broaden the Dartmouth isochrone to generate the template filter at the distance of 8 kpc.**

We generate Hess diagrams of 18 regions each with a $5°$ interval along the $\sim 90°$ GD-1 trace by convolving the SDSS photometric errors on their CMDs. We select the Hess diagrams on which the GD-1 dwarfs obviously overwhelm the background stars as shown in Fig. 10. In each Hess diagram, we shift the filter from -0.3 mag to 0.9 mag in g_0 by the step of 0.01 mag, then use the Equation 2 - 6 in Willett et al. (2009) with assuming the Hess diagram of the background ~ 0 to calculate the distance and error of the region (there is a typos in Equation 6 in Willett et al. (2009), which should be $\sigma_{\delta r} = \sqrt{-\frac{\sigma^2(a)}{a(\delta r_m)\frac{d^2a}{d\delta r^2}}}|_{\delta r=\delta r_m}$, because the second derivative $\frac{d^2a}{d\delta r^2}$ should be not greater than 0 at the maximum). In each panel of Fig. 10, the red line is a Dartmouth isochrone with $[\mathbf{Fe/H}] = -2.3$ and an age of 13 Gyr, and the distance with error is shown in red. All distances with Gaussian errors are listed in Table 1.

2.2. *spectral Data*

We select the GD-1 candidates in the spectral data of SDSS DR14 and LAMOST DR6 by the criteria: (1) $|\varpi| < 1$ mas, (2)$|\phi_2^c| < 1°$, (3) $|\mu_\alpha cos\delta - f_1(\phi_1)| < 2$ mas/yr, (4) $|\mu_\delta - f_2(\phi_1)| < 2$ mas/yr and (5) [Fe/H] < -1.9 dex. For a star that have multiple spectra and multiple measurements, its parameters with errors are the mean values of these measurements. In panel A of Fig. 11, the spectral radial velocities of SDSS DR14 along ϕ_1 are shown by black asterisks, while those of LAMOST DR6 are shown by red circles, and the central red line is

$$f_4(\phi_1) = -273.4 - 6.5 \times \phi_1 \quad (6)$$

km/s, while the dotted lines are $f_4(\phi_1) \pm 50$ km/s. We can see that stars are crowded in this range, where GD-1 members are located. The spectroscopic stars in SDSS DR14 and LAMOST DR6 that meet all of the above four criteria and also have radial velocities $|RV - f_4(\phi_1)| < 50$ km/s are selected as GD-1 spectroscopic stream member candidates. One hundred and thirty-six spectra for 116 individual stars from SDSS DR14 and 32 spectra for 20 individual stars from LAMOST DR6 are given in Table 3 and Table 4 respectively.

Panel B of Fig. 11 shows the [Fe/H] distributions of these spectroscopic member candidates. The black histogram is for SDSS stars, which is fitted by a Gaussian function and indicated by a dotted profile, while the red histogram

is for LAMOST stars. The fitted value of [Fe/H] histogram for SDSS stars is -2.20 ± 0.12 dex, while the peaks of [Fe/H] histograms for SDSS and LAMOST stars are all at ~ -2.25 dex, which are well consistent with -2.3 dex that the photometric data give in Fig. 2. Gao et al. (2015) has shown that for low metal stars, [Fe/H] ((Wu et al. 2014) less than -1.5 dex in LAMOST DR1, which are determined by LASP with ELODIE interpolator) are systematically measured higher when compared with those in the PASTEL catalog(Soubiran et al. 2010). Thus the actual intrinsic metallicity of the GD-1 stream we estimate no more than -2.20 dex, with an estimated error of about 0.12 dex.

Panel C of Fig. 11 shows the sky positions of these candidates, while their CMD is shown in panel D. In these two panels, SDSS stars are indicated by black asterisks, while LAMOST stars are indicated by red circles. The red line in panel D is the Dartmouth isochrone with [Fe/H] $= -2.3$, an age of 13 Gyr, and a distance of 8 kpc. The former panel shows that SDSS stars are distributed along the whole GD-1 trace, while LAMOST stars are only extended to $\phi_1 \sim -52°$ from $\phi_1 \sim 5°$; The latter panel shows most LAMOST stars are giants or subgiants, while SDSS stars are mostly G dwarfs and F turnoff stars.

The parallax distributions of these spectroscopic candidates from SDSS and LAMOST catalogues are shown in panel E by black and red histograms respectively. The parallax distribution of SDSS is fitted by a Gaussian function, which is shown by a dotted profile, with a mean of 0.18 mas and a variance of 0.21 mas. Panel F shows the proper motions of these spectroscopic candidates. The $\mu_\alpha cos\delta$ and μ_δ of SDSS spectroscopic candidates are shown by black asterisks and black crosses respectively, while those of LAMOST spectroscopic candidates are shown by red circles and red diamonds respectively. Equation 2 and 3 are overplotted by black lines as guidelines.

3. ORBIT FITTING

Now we have 6D phase space information along the GD-1 trace: (1) radial velocities from Table 3, 4 and Table 1 in Koposov et al. (2010), (2, 3) proper motions from Equation 2 and 3, (the errors in $\phi_1 : [-60°, -10°]$ are less than 0.4 mas/yr, beyond this range the errors are harder to estimated, but we estimate a large upper bound of 1 mas/yr), (4) the isochrone fitting distances from Table 1 and (5, 6) the sky positions from Table 2. We use three Galactic potential models from $galpy$[3](Bovy 2015) to fit the GD-1 trace: Model 1 is a spherical $MWPotential2014$, Model 2 is $LogarithmicHaloPotential$ with the potential flattening $q_\Phi = 0.9$, the distance from the sun to the Galactic center $ro = 8.0$ kpc and the circular velocity at sun $vo = 220$ km/s, and Model 3 is similar to Model 2 but $ro = 8.5$ kpc.

We construct an objective function of how well each model fits based on 6D information. The objective function is defined as the sum of χ^2 of each dimension divided by the number of data points (data of five of the six dimensions are functions of ϕ_1). The χ^2 of each dimension is the sum of squares of differences between data and modal divided by the data errors. We minimize the value of the objective function, then obtain the GD-1 orbit under a given modal. Results are shown in Fig. 12. The red data are from this paper, while the blue data are from Koposov et al. (2010). The red data and blue radial velocities are used to fit the GD-1 orbit by models, while other blue data are used for comparison. The dashed dotted, dashed and solid lines are the fitted orbits from Model 1, 2 and 3 respectively. From this figure, and the extended, added data gather here, we find the data can be well fitted by Models 2 and 3, while Model 1 has a much poorer fit. The orbit from Model 3 shows that the stream has an eccentricity $e \sim 0.3$, perigalacticon of 14.2 kpc, apogalacticon of 27.0 kpc and inclination approximately $i \sim 40°$.

4. DISCUSSION

In this section, we continue to inspect the GD-1 stream and its environs. We select stars by criteria: (1) $|\varpi| < 1$ mas, (2) $|\mu_\alpha cos\delta - f_1(\phi_1)| < 2$ mas/yr, (3) $|\mu_\delta - f_2(\phi_1)| < 2$ mas/yr, (4) $-85° < \phi_1 < 5°$, and (5) $-0.4 < gr_0 < 1.1$. We use

$$D(\phi_1) = 10.4 + 0.105 \times \phi_1 + 0.00103 \times \phi_1^2 \tag{7}$$

(in kpc) to fit the distance given by Modal 3 in Section 3 along the GD-1 trace, with error less than 0.1 kpc. Then we shift all stars to 8 kpc by distance modulus $DM = 5 \lg(D(\phi_1)/8)$ and denote $g_0^c = g_0 - DM$. We also obtain the absolute magnitude of SDSS g: $M_g = g_0 - 5 \lg(D(\phi_1)) - 10$. We will use the refined magnitude definition here in the section that follows to explore density variation along the stream.

4.1. *Stellar Density Fluctuation along the GD-1 Trace*

---

[3] http://github.com/jobovy/galpy

In this refined CMD (in (gr_0, g_0^c) coordinates), we use Equation 1 to select GD-1 dwarfs, where g_0 is replaced by g_0^c. The sky positions of these dwarfs are shown in the upper panel of Fig. 13, where the blue line is $\phi_2^c = 0°$ and the blue dotted lines are $\phi_2^c = \pm 0.5°$. The stellar counts with Poisson error along GD-1 trace between the two blue dotted lines are shown in the bottom panel. While we acknowledge that because we use Gaia DR2 to select candidate stream members, and that catalog is limited to $g \sim 21$, that the statistical significance of suspect over or underdensities may also be limited, we do find that:

(1) There are four candidate overdensities along the GD-1 trace. These four overdensities are at ϕ_1 : $[-54°, -43°]$, $[-37°, -23°]$, $[-17°, -11°]$ and $[-3°, 2°]$, which are denoted as O1, O2, O3 and O4 respectively;

(2) There is a gap centered around $\phi_1 \sim -21°$, which has no GD-1 candidate member star;

(3) There are two candidate underdensitiies at $\phi_1 \sim -40°$ and $\phi_1 \sim -8°$;

(4) The width of stream visually broadens along the GD-1 trace from O3 along two directions;

(5) There is a noticeable wobble in O1;

(6) The stellar density drops suddenly to background level at $\phi_1 \sim 2°$;

(7) A spur originates at $\phi_1 \sim -40°$, where the O1 and O2 are separated, which is discussed by Price-Whelan & Bonaca (2018) and also shown in Figure 10 of Koposov et al. (2010). We conjecture that it results from GD-1 stars pulled out of the stream by an encounter. Thus, O1 and O2 were once on a single overdensity, but separated later.

Fig. 14 shows the density profiles of four overdensities O1, O2, O3 and O4 along ϕ_2^c. We fit these profiles by Gaussian functions, and in each panel, the Gaussian width σ, center and full width at half maximums(FWHM) are also given in red. Their lengths along ϕ_1 and FWHMs in degrees along the ϕ_2^c are shown by the red rectangles in the upper panel of Figure 13. All information about these four overdensities are given in Table 5, where the areal densities of dwarfs are the ratios of dwarf number(calculated from Gaussian fitting) divided by areas of rectangles in the upper panel of Fig. 13. Their Gaussian centers are $0.039°, -0.051°, 0.147°$ and $-0.115°$ in ϕ_2^c respectively, while Gaussian widths are $0.290°, 0.147°, 0.119°$ and $0.247°$ respectively, which correspond to FWHMs of 91.9 pc, 49.4 pc, 44.6 pc and 104.7 pc respectively by the distance of Equation 7. These FWHMs show that the narrowest place of the GD-1 stream is in O3, and then broadens gradually along two directions. Besides, O3 has the highest areal density of dwarfs as shown in Table 5. For stars stripped from the progenitor cluster earlier would move away further both in position and velocity from the progenitor(Bovy et al. 2014). So O3 centered $(\phi_1, \phi_2^c) \sim (-14°, 0.15°)((\alpha, \delta) \sim (178.18°, 52.19°))$, which has the narrowest stream width, highest stellar areal density and also shows a noticeable wobble, is the most likely candidate for the GD-1 stream progenitor.

Systems at the end of their bound lifetime like GD-1 are not expected to be stripped smoothly, so at least some fluctuations from the normal trace are expected to simply be the result of the last few stripping episodes being stochastic and erratic. But given the overall density structure, it seems possible that the local density is affected by the encounters that created the under dense features. After all, the energy of the stars is redistributed, and shocks and caustics could mess up the smooth stream density. A more detailed dynamical model of the stream over time including encounters with dense structures and tracing the stream as it passes through the plane of the disk will help determine the nature of these encounters.

4.2. *Blue Horizontal Branch(BHB) Stars and Blue Stragglers(BS)*

In this subsection, we require selected stars satisfying the following criteria: (1) $|\varpi| < 1$ mas; (2) $-85° < \phi_1 < 5°$; (3) $|\mu_\alpha cos\delta - f_1(\phi_1)| < 2$ mas/yr; (4) $|\mu_\delta - f_2(\phi_1)| < 2$ mas/yr; (5) $-1° < \phi_2^c < 1°$. Their CMD is shown in Fig. 15.

Because the spectroscopic parameters for hot stars are more difficult to derive, due to less characteristic spectral lines, different physical mechanism and sparse templates, we only give radial velocities for stars with $gr_0 < 0.1$ from LAMOST DR6 and SDSS DR14, which are shown in Fig. 16, where one symbol represent one spectrum, so a star may have several symbols. From the figure we can see that the radial velocities of all blue stars are well within the radial velocity range of GD-1 stream, so we believe all these spectroscopically observed stars are GD-1 members. All blue stars with $gr_0 < 0.1$ from spectroscopic catalogues of LAMOST DR6 and SDSS DR14 are listed in Table 6 and Table 7 respectively.

We overplot all spectroscopic GD1 member stars from LAMOST DR6 and SDSS DR14 by red and blue circles in Fig. 15 respectively – the positions of BHB and BS stars of the GD-1 stream are clearly shown. We select BHB stars by the criteria of $0.3 < M_g < 0.8$ and $-0.3 < gr_0 < -0.1$, and BS stars by the criteria of $1.5 < M_g < 4$ and $-0.2 < gr_0 < 0.1$. There are total seven BHB and 21 BS stars of the GD-1 stream, which are listed in Table 8. In LAMOST DR6 and SDSS DR14, there are six and two spectroscopic BHB stars respectively, and four and eight

Table 1. Circle centers in Fig. 4 and distances in Fig. 10

ϕ_1 range [deg]	$(\mu_\alpha cos\delta, \mu_\delta)$ [mas/yr]	distance [kpc]
$[-85, -80]$	$(-2.2, -10.0)$	8.5 ± 0.1
$[-80, -75]$	$(-2.4, -10.7)$	
$[-75, -70]$	$(-2.4, -11.2)$	
$[-70, -65]$	$(-2.8, -12.0)$	
$[-65, -60]$	$(-3.5, -12.6)$	8.0 ± 0.4
$[-60, -55]$	$(-4.2, -13.0)$	8.0 ± 0.2
$[-55, -50]$	$(-4.4, -13.0)$	7.6 ± 0.1
$[-50, -45]$	$(-4.8, -12.8)$	8.0 ± 0.1
$[-45, -40]$	$(-5.4, -12.8)$	8.0 ± 0.2
$[-40, -35]$	$(-5.8, -12.6)$	8.6 ± 0.2
$[-35, -30]$	$(-6.3, -11.7)$	8.5 ± 0.2
$[-30, -25]$	$(-6.9, -11.0)$	8.0 ± 0.2
$[-25, -20]$	$(-7.0, -10.2)$	8.5 ± 0.1
$[-20, -15]$	$(-7.5, -8.7)$	9.2 ± 0.1
$[-15, -10]$	$(-7.9, -7.6)$	9.2 ± 0.1
$[-10, -5]$	$(-8.5, -6.0)$	9.7 ± 0.4
$[-5, 0]$	$(-8.0, -4.4)$	10.4 ± 0.2
$[0, 5]$	$(-7.6, -3.3)$	

spectroscopic BS stars respectively. Not counting spectra of the same star, we have a total of six new spectroscopic BHB and ten new spectroscopic BS candidate stream members.

5. CONCLUSION

In this paper, combining spectroscopic and photometric data from SDSS DR14, high precision astrometric data from Gaia DR2 and spectroscopic data from LAMOST DR6, add significantly to the numbers of GD-1 stream high confidence candidate members and obtain a full 6D phase-space map of GD-1 stream with high precision. We conclude this information about the GD-1 steam and its stellar contents:

(1) The GD-1 stream is the relic of a very old, low dispersion object, such as a metal-poor globular cluster or possibly an ultra-faint dwarf galaxy, with [Fe/H] ~ -2.3.

(2) Its observed length today on the sky from the sun is at least $90°$.

(3) There are four candidate stellar overdensities, one candidate gap and two candidate stellar underdensities along the stream trace. The trace appears to break at $\phi_1 = 2°$.

(4) The GD-1 progenitor is most likely located at $(\phi_1, \phi_2^c) \sim (-14°, 0.15°)$(i.e. $(\alpha, \delta) \sim (178.18°, 52.19°)$).

(5) A spur originating about $\phi_1 \sim -40°$ seems to consist stream stars pulled off from the GD-1 stream by an encounter with a massive object.

(6) We find six new BHB and 10 BS spectroscopic members of GD-1.

In summary, thanks to Gaia DR2, we can obtain much detailed phase space information about the GD-1 stream, which can help us to explore the nature of GD-1 stream and study the Galactic potential. The spectra of stream members from SDSS DR14 and LAMOST DR6 helps to understand the origin of the progenitor of the GD-1 stream. Four apparent overdensities, the gap, the spur, and other stellar fluctuations along the stream can help us to understand the history of GD-1 disruption process and possibly the nature and frequency of massive dark matter subhalo encounters.
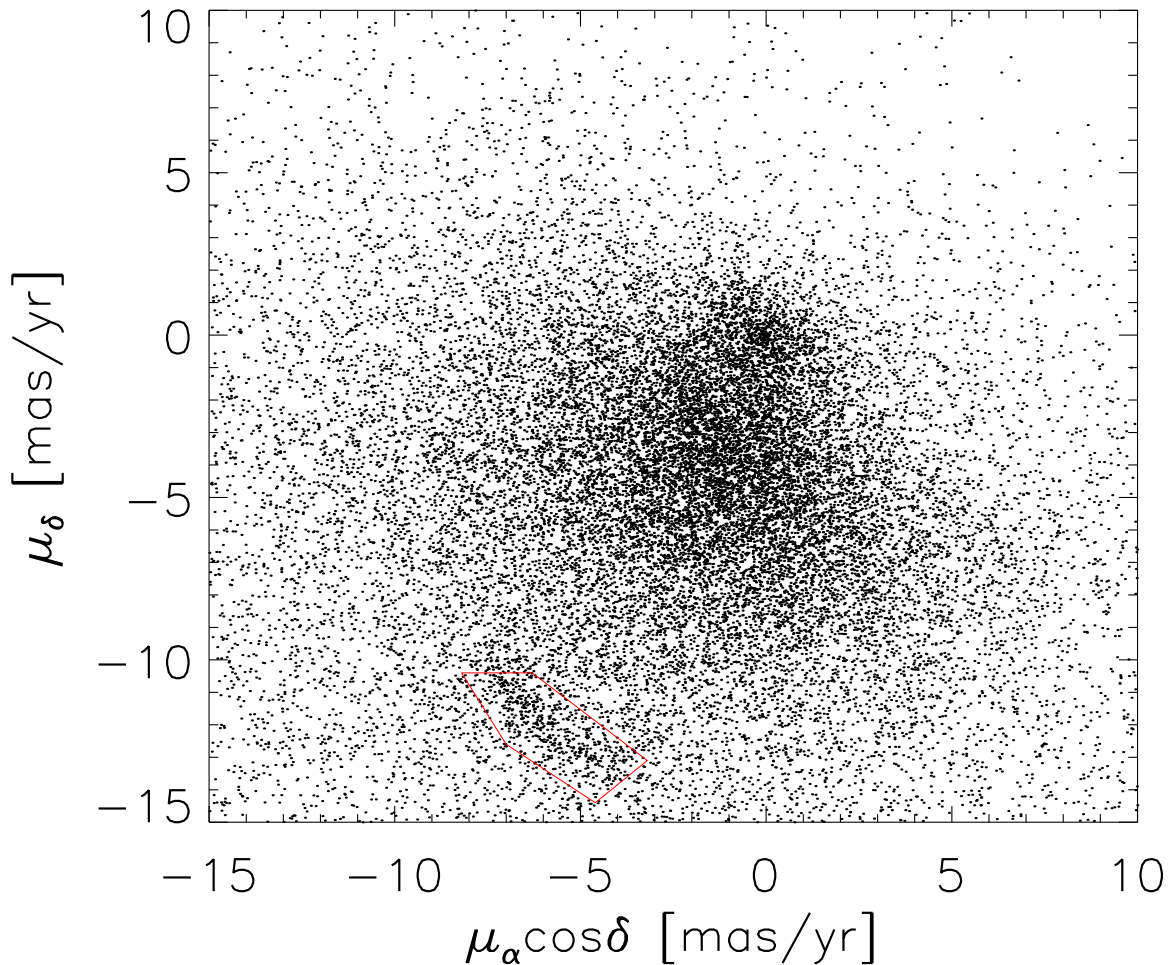
Figure 1. The proper motions of stars within $-60° < \phi_1 < -20°$ and $-0.2° < \phi_2 < 0.2°$. The red polygon is the region where we select GD-1 member candidates.

Guoshoujing Telescope (the Large Sky Area Multi-Object Fiber Spectroscopic Telescope LAMOST) is a National Major Scientific Project built by the Chinese Academy of Sciences. Funding for the project has been provided by the National Development and Reform Commission. LAMOST is operated and managed by the National Astronomical Observatories, Chinese Academy of Sciences.

Software: galpy (Bovy 2015); TopCat (Taylor 2005)

REFERENCES

Bovy, J. 2014, ApJ, 795, 95

Bovy, J., Bahmanyar, A., Fritz, T. K., & Kallivayalil, N. 2016, ApJ, 833, 31

Bovy, J. 2015, ApJS, 216, 29

Bowden, A., Belokurov, V., & Evans, N. W. 2015, MNRAS, 449, 1391

Carlberg, R. G., & Grillmair, C. J. 2013, ApJ, 768, 171

Carlberg, R. G. 2016, ApJ, 820, 45

Cui, X.-Q., Zhao, Y.-H., Chu, Y.-Q., et al. 2012, Research in Astronomy and Astrophysics, 12, 1197

de Boer, T. J. L., Belokurov, V., Koposov, S. E., et al. 2018, MNRAS, 477, 1893

Dotter, A., Chaboyer, B., Jevremović, D., et al. 2008, ApJS, 178, 89

Huang, Y., Liu, X.-W., Chen, B.-Q., et al. 2018, arXiv:1806.03748

Gaia Collaboration, et al. 2018, arXiv:1804.09365

Gao, H., Zhang, H.-W., Xiang, M.-S., et al. 2015, Research in Astronomy and Astrophysics, 15, 2204

Grillmair, C. J., & Dionatos, O. 2006, ApJL, 643, L17
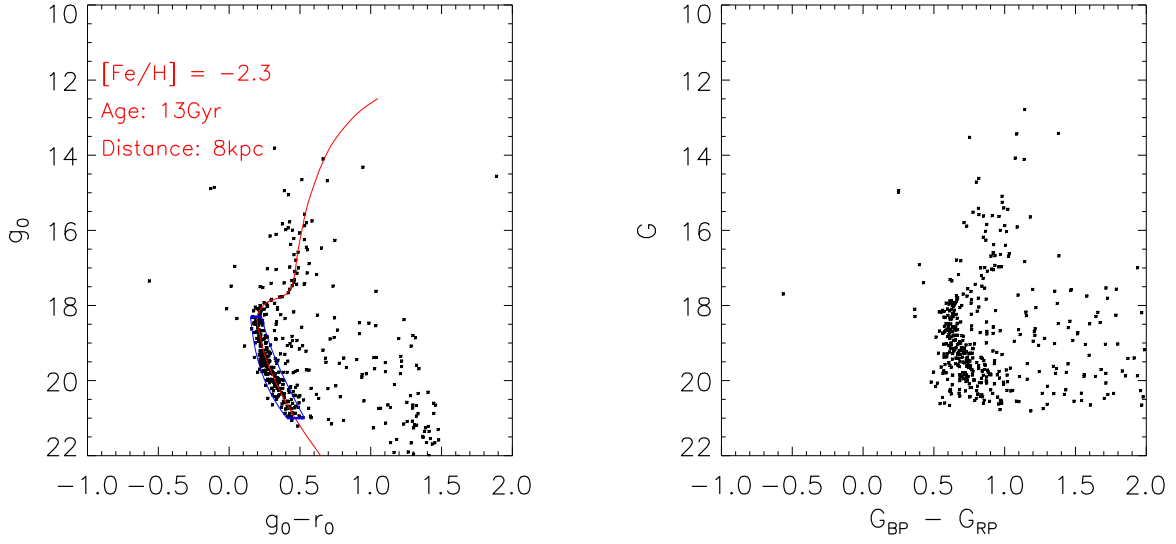
Figure 2. The CMDs of GD-1 stars in the red polygon in Fig. 1. Light panel: The CMD is from SDSS DR9. The red line is the isochrone with [Fe/H]= −2.3, an age of 13 Gyr and a distance of 8 kpc. Right panel: The CMD is from Gaia DR2. The G, G_{BP}, and G_{RP} are the three broad-band magnitudes of Gaia DR2 without correction for extinction.
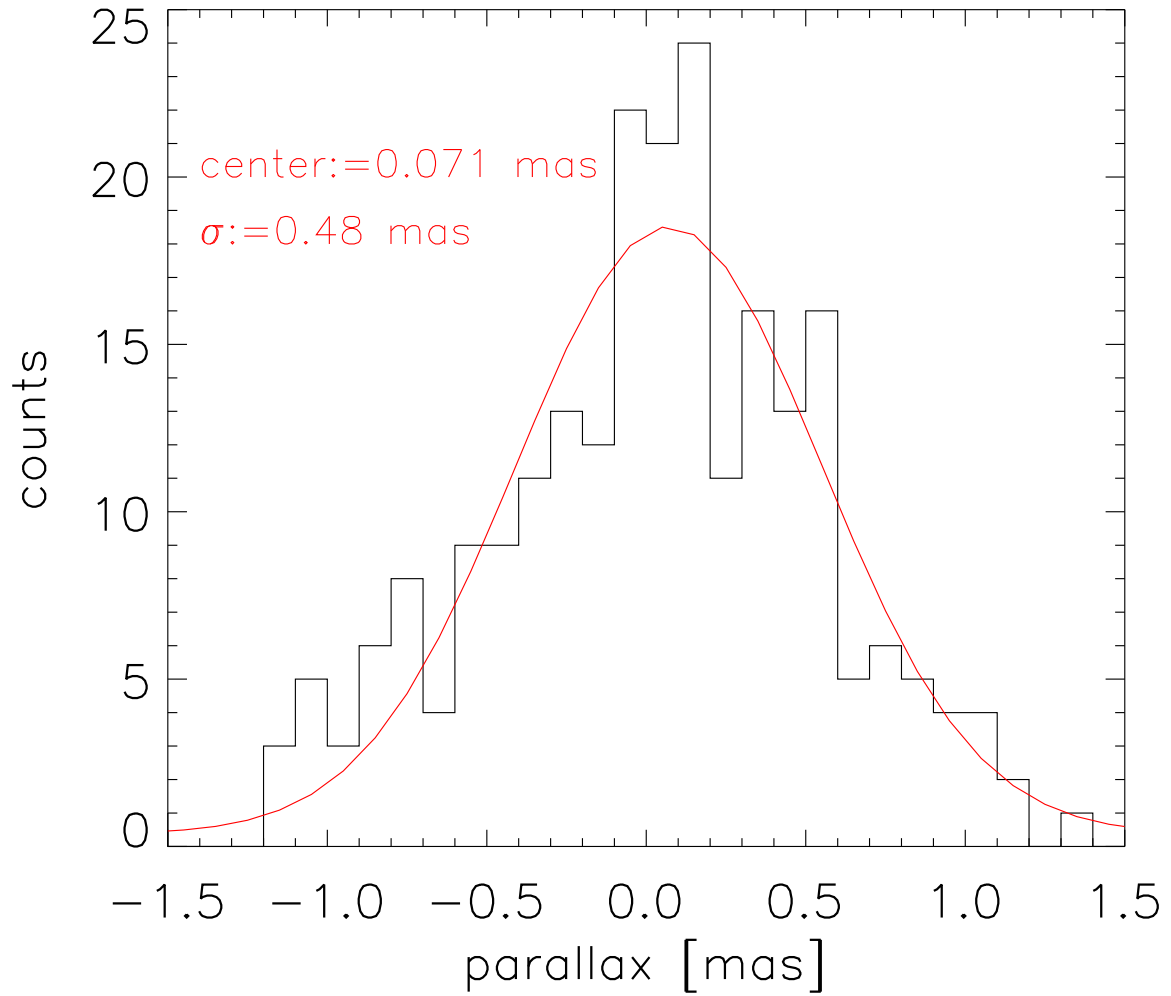
Figure 3. The parallax distribution of GD-1 stars enclosed by blue lines in Fig. 2.
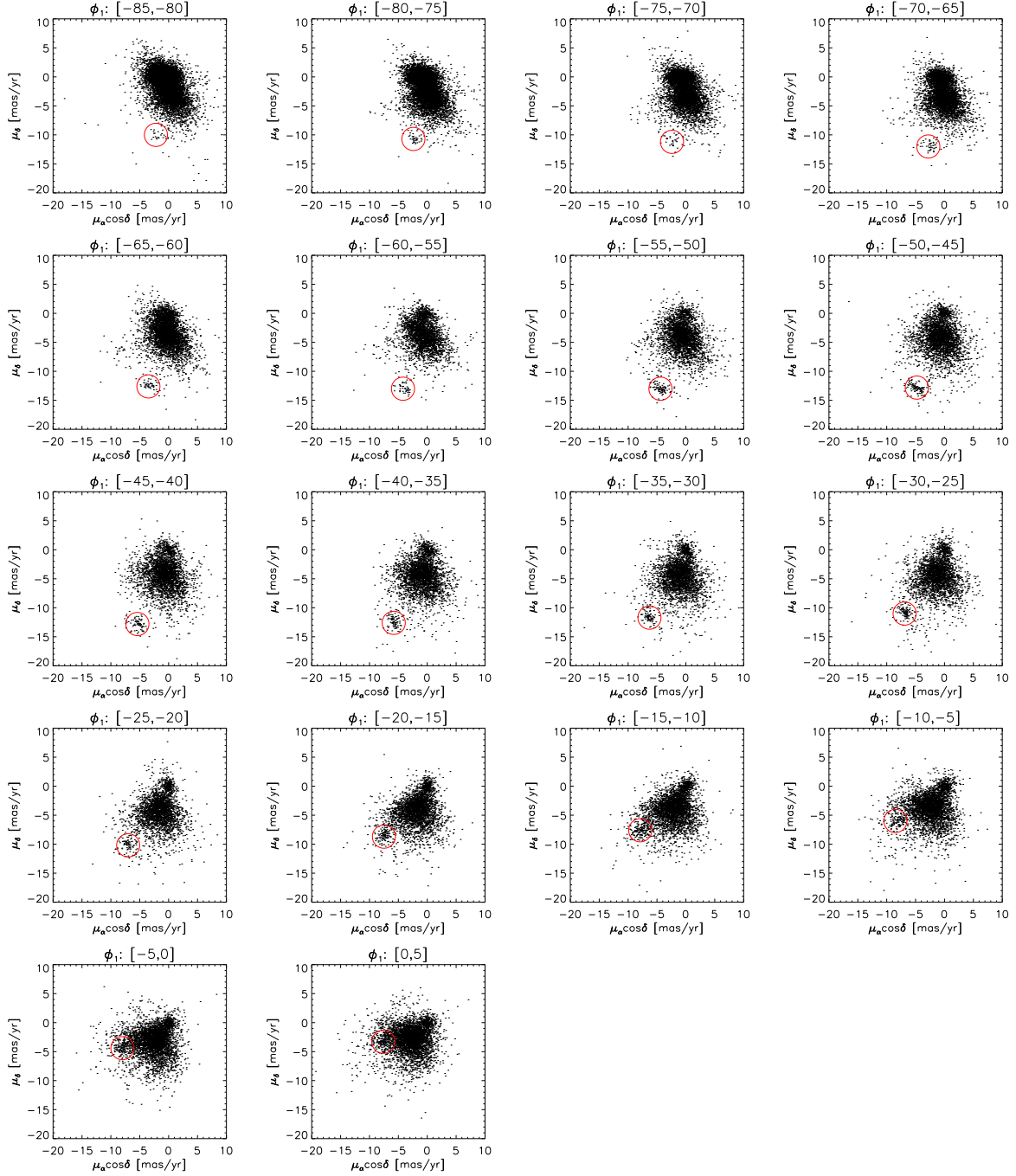
Figure 4. The proper motions of stars selected by the CMD of GD-1 dwarf stars with $|\varpi| < 1$ mas, $-5° < \phi_2 < 1°$ and distances within $8 - 10$ kpc. The ϕ_1 range of each panel is give in the title. The red circle in each panel is the range where we select GD-1 candidates. Their centers are given in Table 1, and radii are all 2 mas/yr.
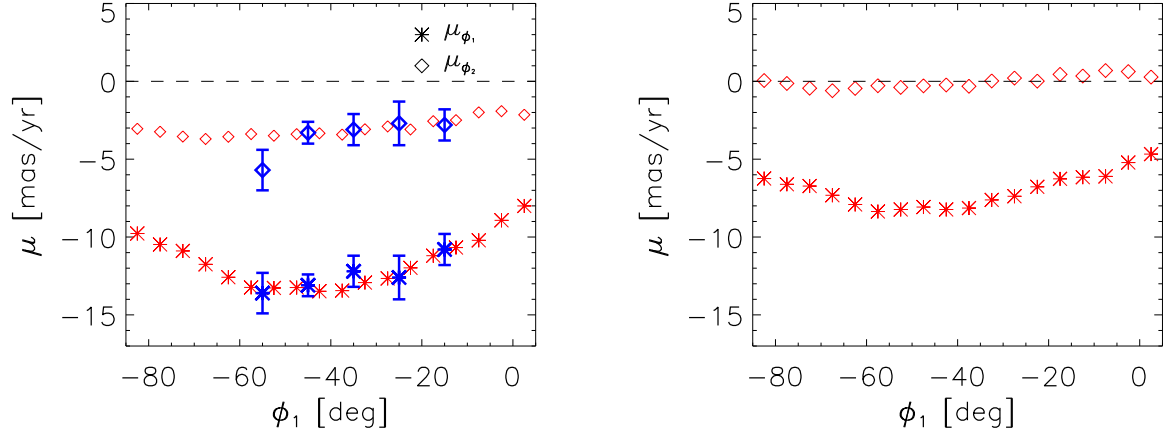
Figure 5. The circle centers in Fig. 4, but have been converted to (ϕ_1, μ) coordinate. In each panel, circles are μ_{ϕ_1}s, while diamonds are μ_{ϕ_2}s, and the data from Table 1 are shown in red, while those from Table 4 in Koposov et al. (2010) are shown in blue. The proper motions in the right panel have been corrected for the Sun's reflex motion, while those in the left panel are not corrected.
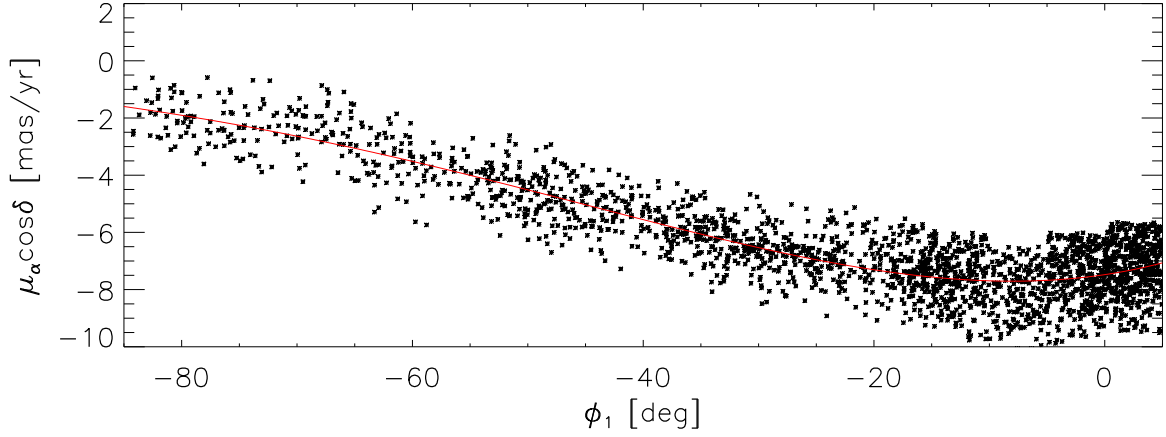
Figure 6. The relationship between Gaia $\mu_\alpha cos\delta$ and ϕ_1. The red line is Equation 2.
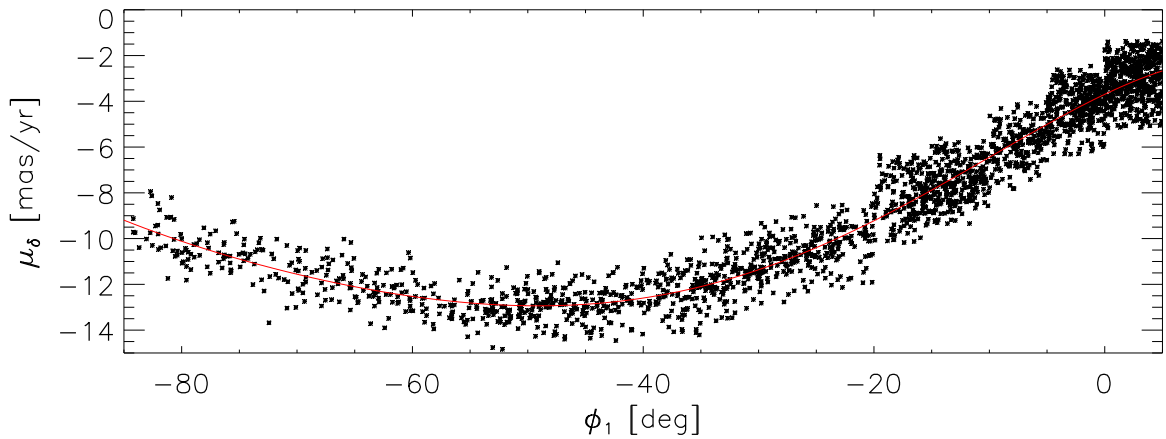
Figure 7. The relationship between Gaia μ_δ and ϕ_1. The red line is Equation 3.
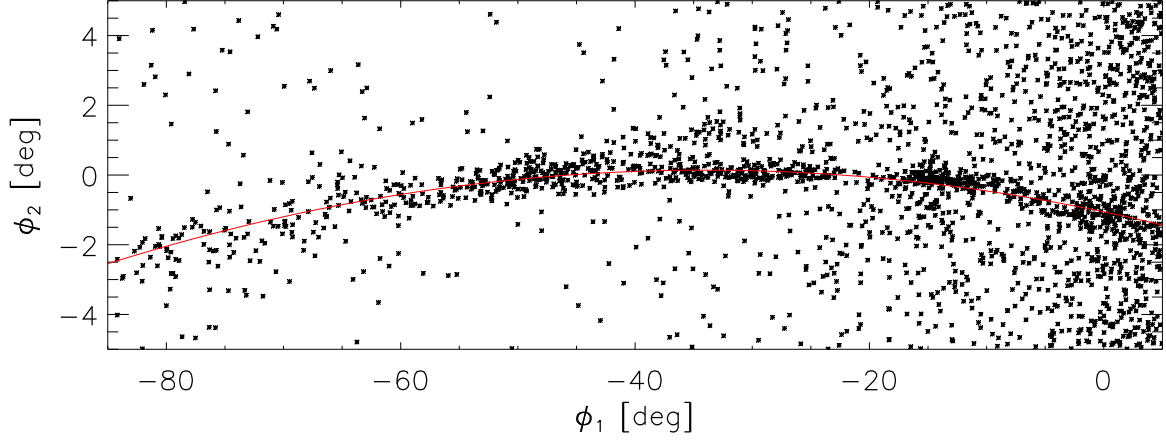
Figure 8. Positions of all stars in the red circles in Fig. 4. The red line is the Equation 4.
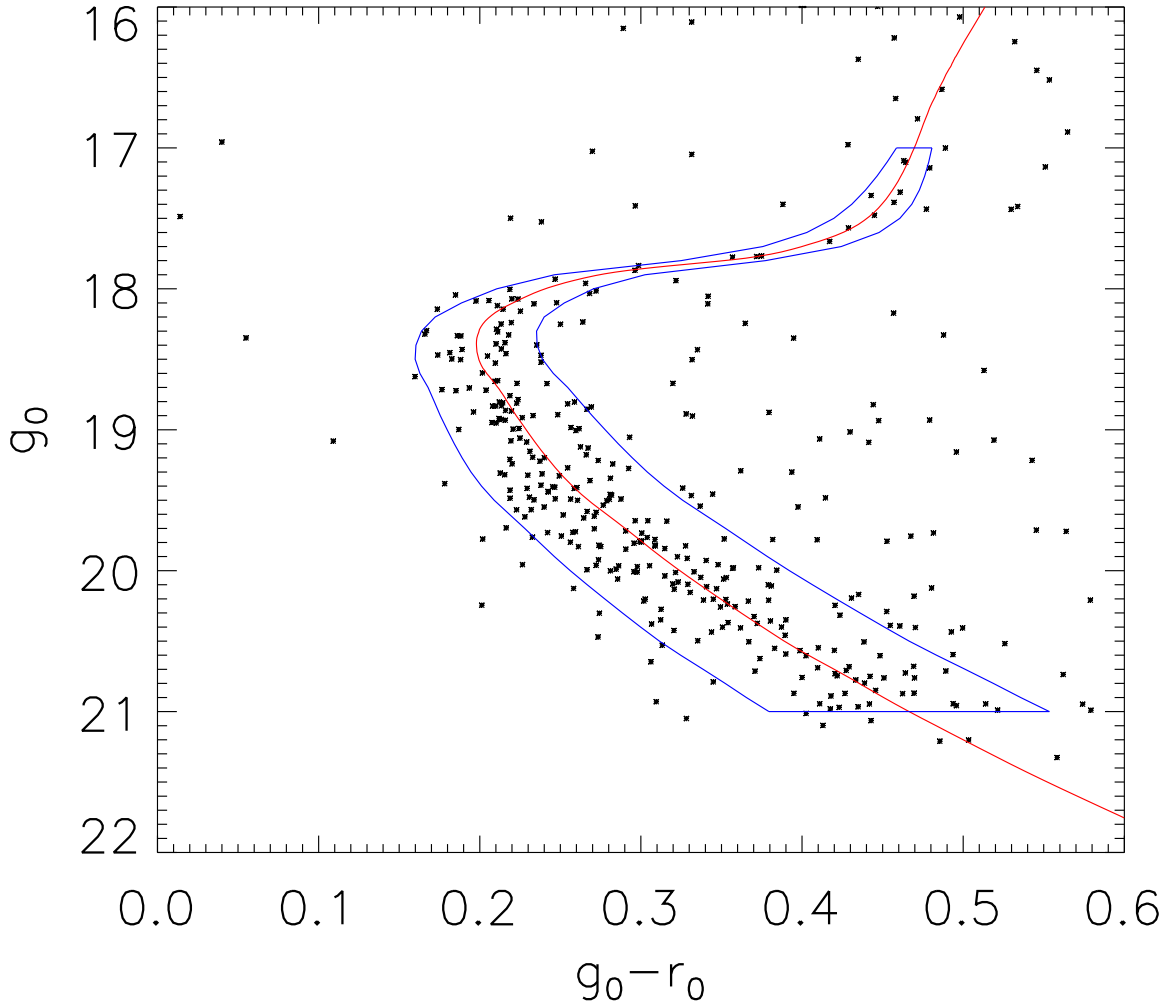
Figure 9. The twice $\sigma(g_0)$, which is used to broaden the Dartmouth isochrone between $17 < g_0 < 21$ to generate the template filter, is shown by blue lines. The stars in Fig. 2 are shown by black symbols. The red line is the Dartmouth isochrone with [Fe/H]$= -2.3$, an age of 13 Gyr and a distance of 8 kpc.
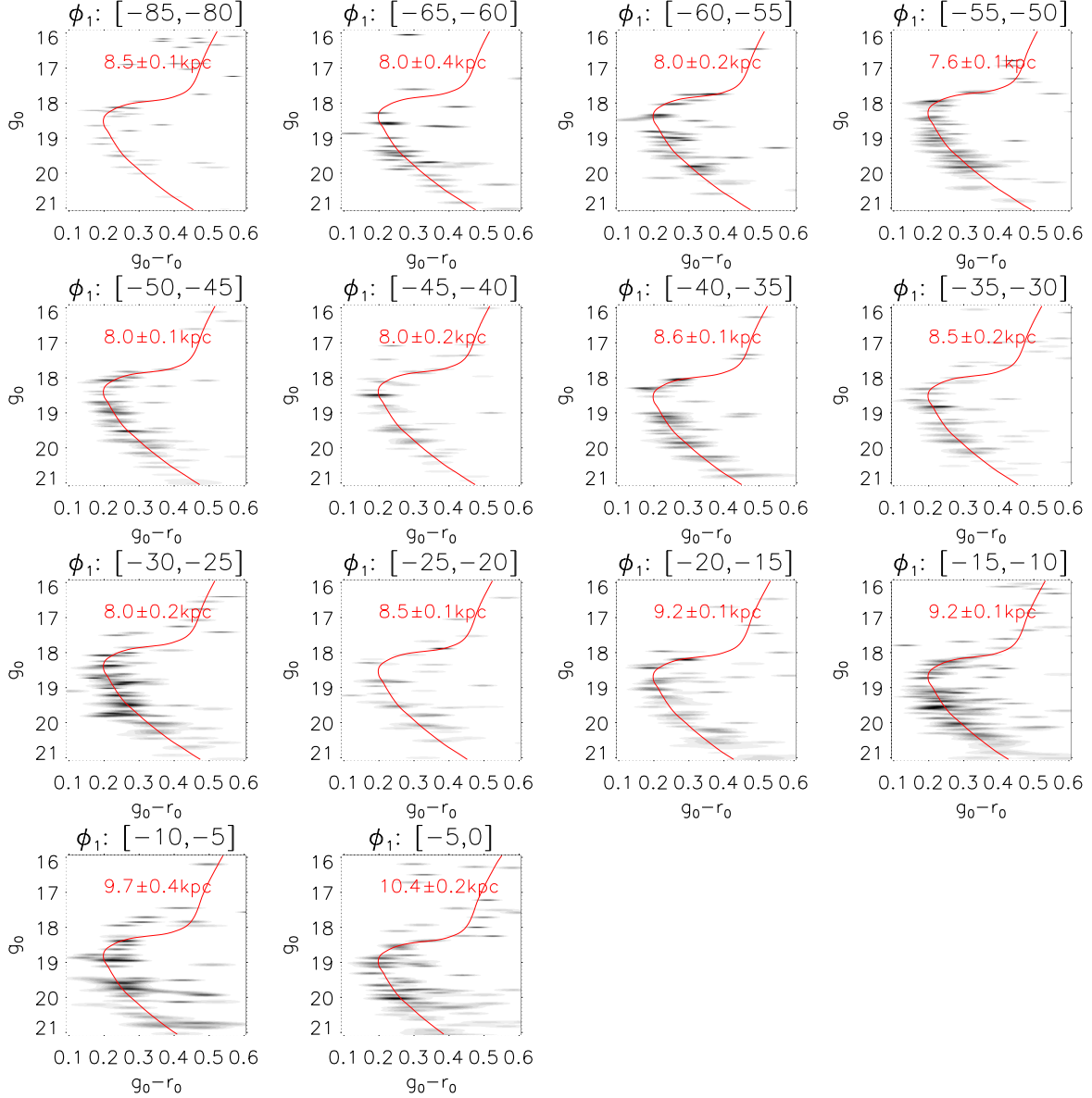
Figure 10. The Hess diagrams of 14 regions along the GD-1 trace. In each panel, the red line is the isochrone with [Fe/H] $= -2.3$ and an age of 13 Gyr, and the distance with error is given by the red number.

Koleva, M., Prugniel, P., Ocvirk, P., Le Borgne, D., & Soubiran, C. 2008, MNRAS, 385, 1998

Koleva, M., Prugniel, P., Bouchard, A., & Wu, Y. 2009, A&A, 501, 1269

Koposov, S. E., Rix, H.-W., & Hogg, D. W. 2010, ApJ, 712, 260

Lindegren, L., et al. 2018, arXiv:1804.09366

Price-Whelan, A. M. & Bonaca, A. 2018, arXiv:1805.00425

Schlafly, E. F., & Finkbeiner, D. P. 2011, ApJ, 737, 103

Schlegel, D. J., Finkbeiner, D. P., & Davis, M. 1998, ApJ, 500, 525

Soubiran, C., Le Campion, J.-F., Cayrel de Strobel, G., & Caillo, A. 2010, A&A, 515, A111

Stassun, K. G. & Torres, G. 2018, arXiv:1805.03526

Taylor, M. B. 2005, Astronomical Data Analysis Software and Systems XIV, 347, 29

Willett, B. A., Newberg, H. J., Zhang, H., Yanny, B., & Beers, T. C. 2009, ApJ, 697, 207

Wu, Y., Luo, A.-L., Li, H.-N., et al. 2011, Research in Astronomy and Astrophysics, 11, 924

Wu, Y., Singh, H. P., Prugniel, P., Gupta, R., & Koleva, M. 2011, A&A, 525, A71

Wu, Y., Du, B., Luo, A., Zhao, Y., & Yuan, H. 2014, Statistical Challenges in 21st Century Cosmology, 306, 340
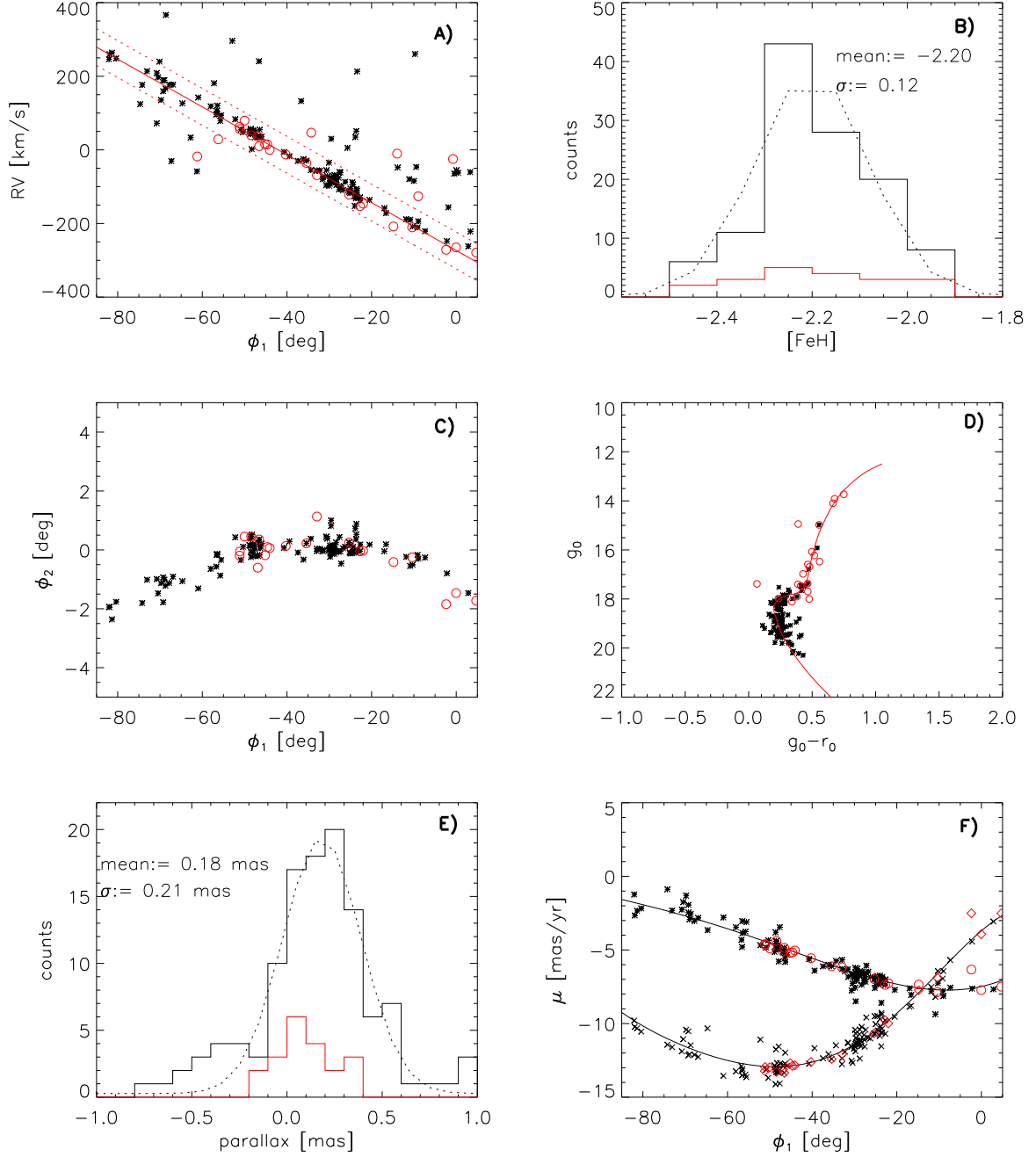
Figure 11. The GD-1 candidates in the spectroscopic data of SDSS DR14 and LAMOST DR6 satisfying the criteria: (1) $|\varpi| < 1$ mas, (2)$|\phi_2^c| < 1°$, (3) $|\mu_\alpha cos\delta - f_1(\phi_1)| < 2$ mas/yr, (4) $|\mu_\delta - f_2(\phi_1)| < 2$ mas/yr and (5) [Fe/H] < -1.9 dex. Their radial velocities are shown in panel A. The [Fe/H] distributions, sky positions, CMD, parallax distributions and proper motions of the stars within $|RV - f_4(\phi_1)| < 50$ km/s are shown in panel B, C, D, E, and F respectively. The red symbols and histograms are for the LAMOST stars, while black symbols and histograms are for the SDSS stars.
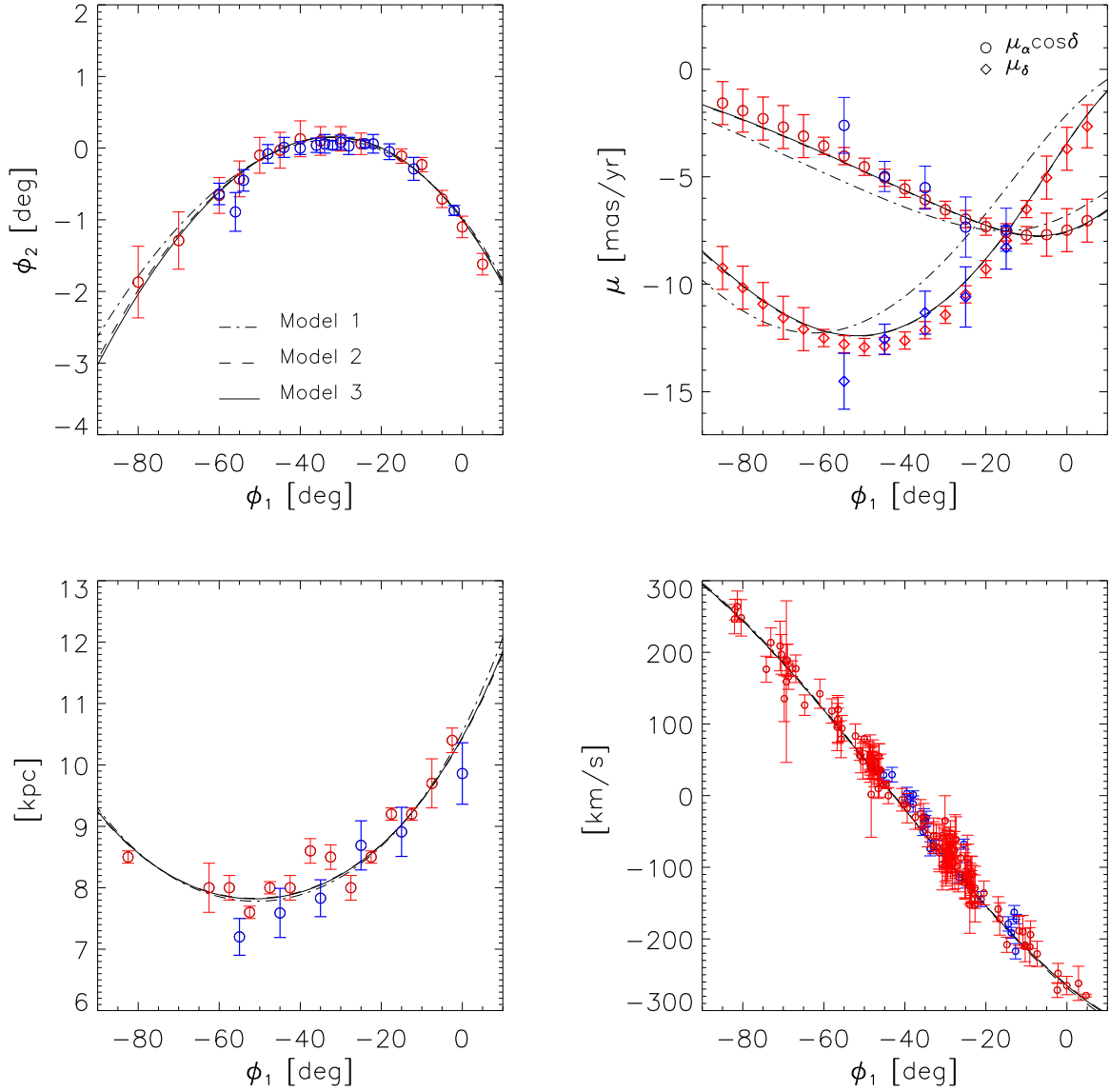
Figure 12. The fitted orbits by three models. The red data are from this paper, while the blue data are from Koposov et al. (2010). The red data and blue radial velocities are used to fit the GD-1 orbits by models, while other blue data are used for comparison. The dashed dotted, dashed and solid lines are the fitted orbits from Model 1, 2 and 3 respectively.
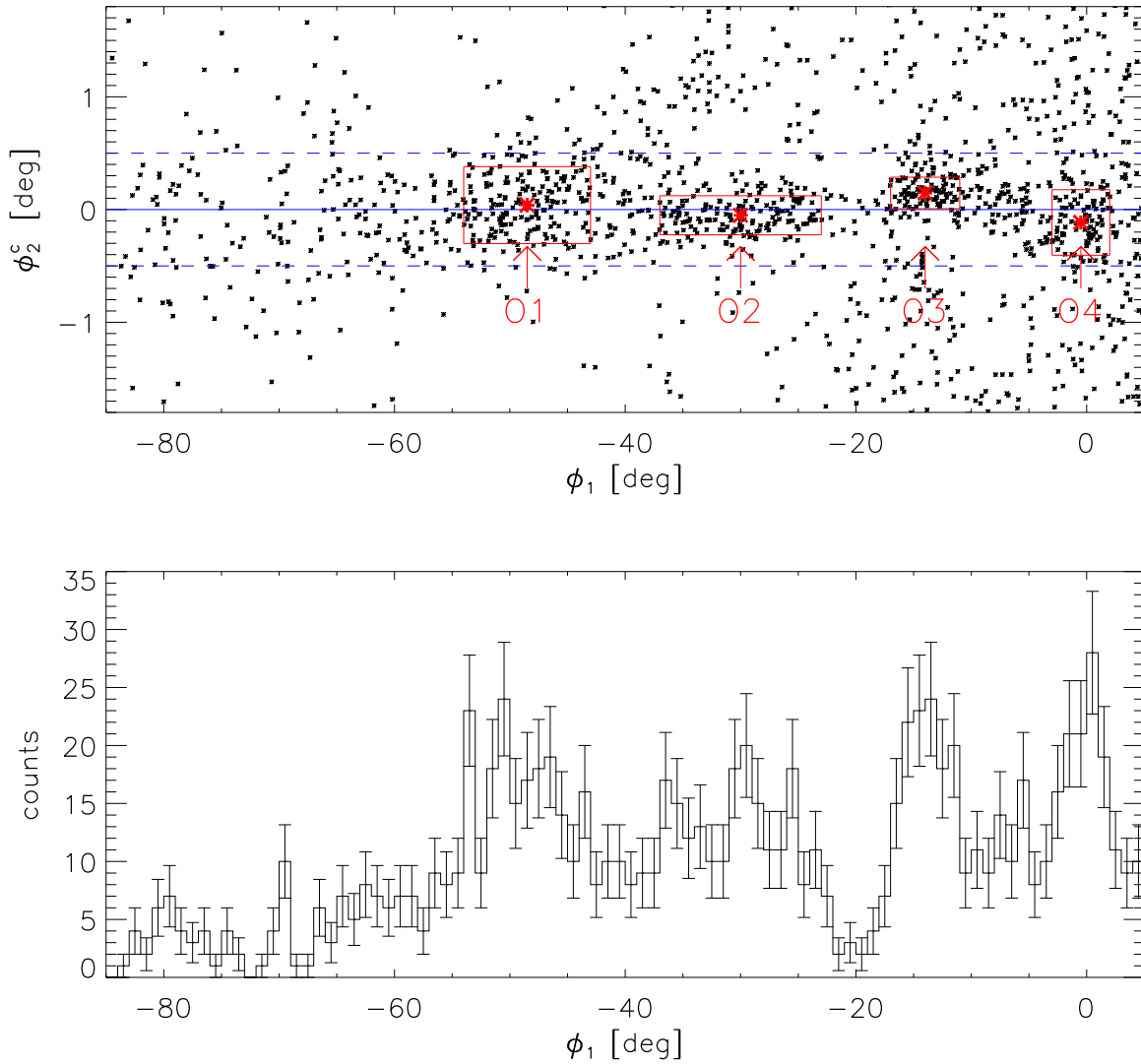
Figure 13. Upper panel: The sky positions of stars selected by Equation 1, where g_0 is replaced by g_0^c. The blue line is $\phi_2^c = 0°$, while the blue dotted lines are $\phi_2^c = \pm 0.5°$. Bottom panel: The stellar density histogram with Poisson error along the GD-1 trace within two blue dashed lines in the upper panel.

Yanny, B., Rockosi, C., Newberg, H. J., et al. 2009, AJ, 137, 4377

Zinn, J. C., Pinsonneault, M. H., Huber, D, & Stello, D. 2018 arXiv:1805.02650

Zhao, G., Zhao, Y.-H., Chu, Y.-Q., Jing, Y.-P., & Deng, L.-C. 2012, Research in Astronomy and Astrophysics, 12, 723
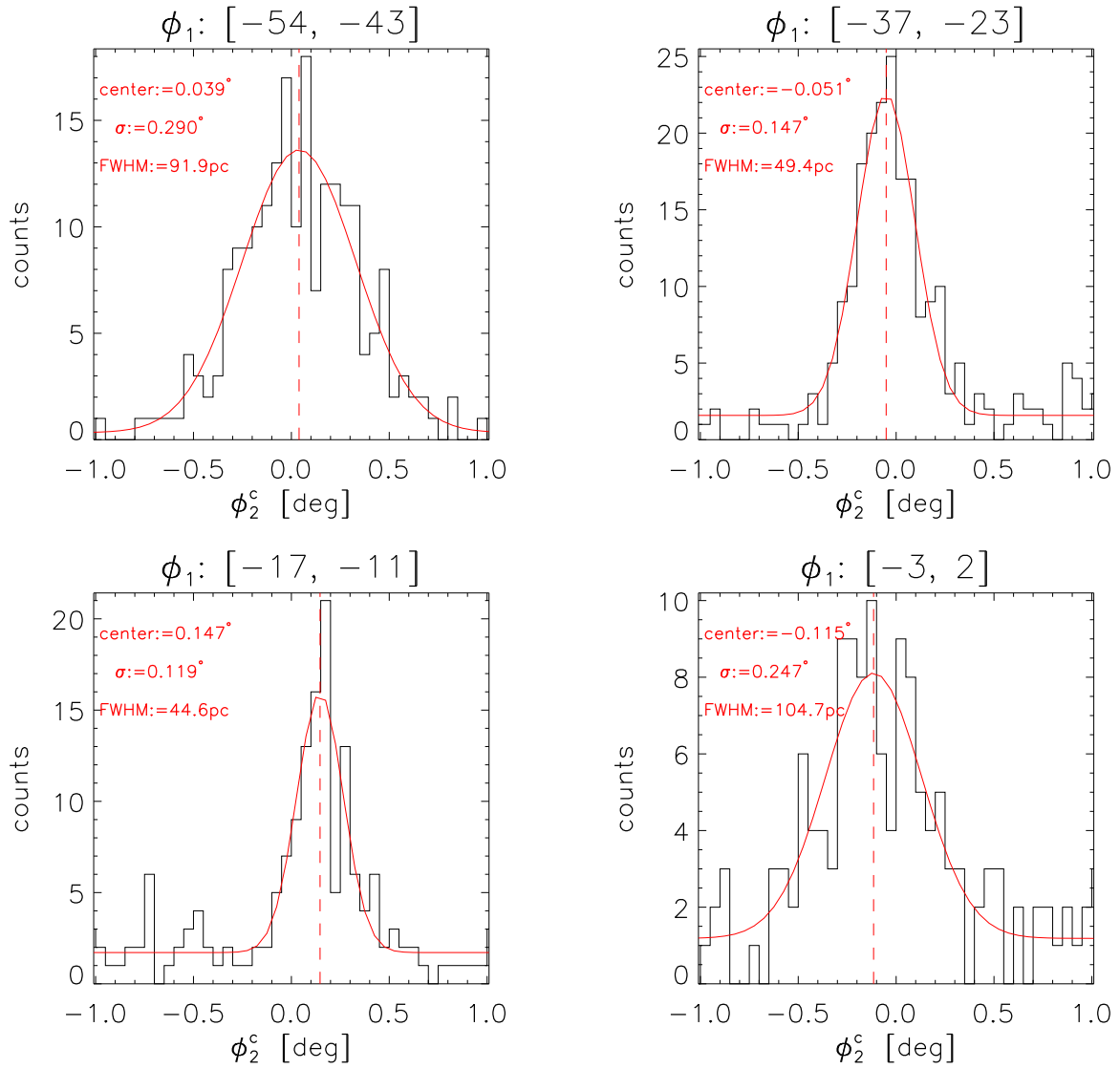
Figure 14. Stellar density profiles for four overdensities. The fitted Gaussian functions are overplotted on the histograms by red lines, and the fitted centers and dispersions are also given.
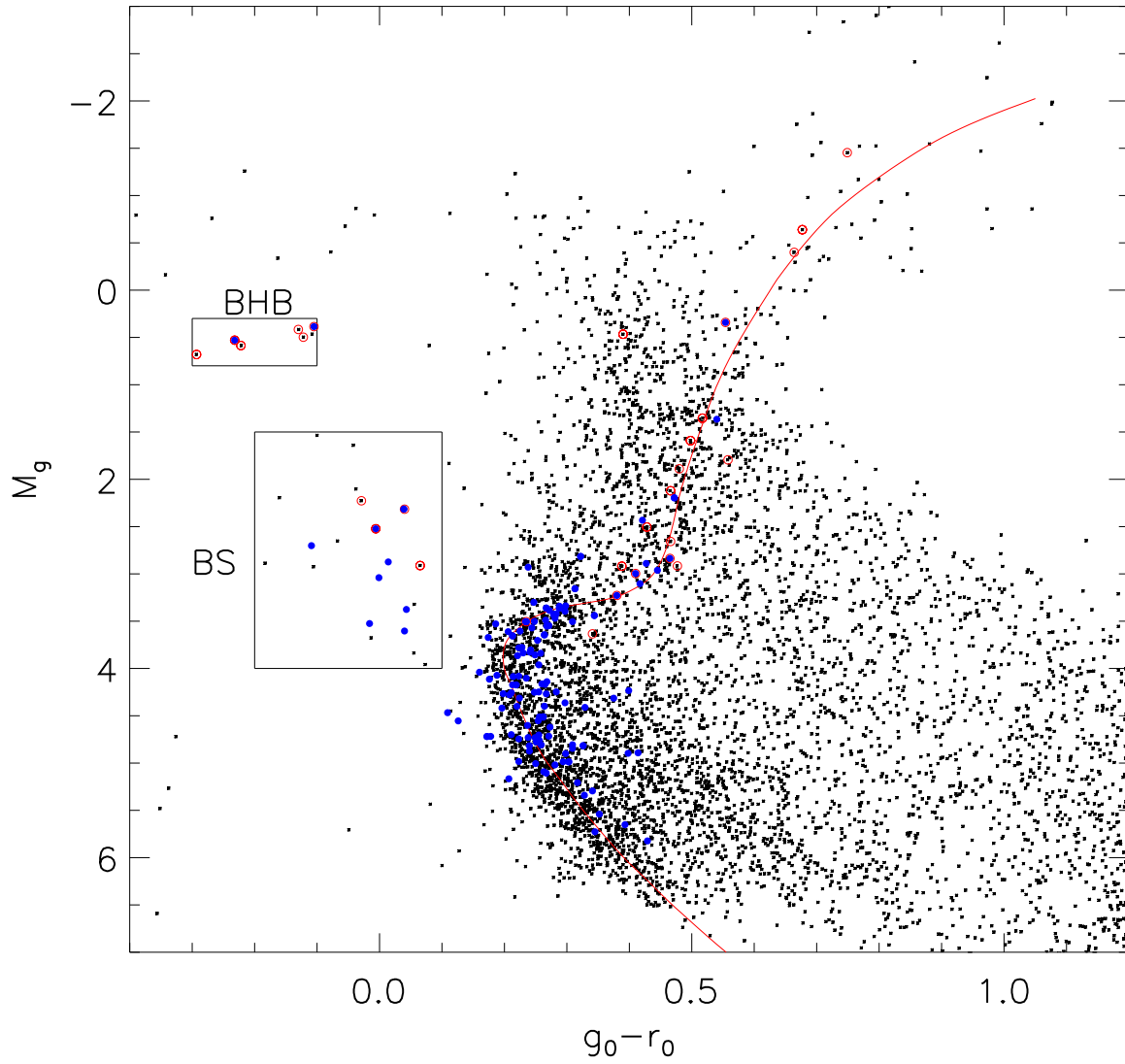
Figure 15. Stars are selected by the criteria in Section 4.2. The red curve is the isochrone with [Fe/H] = −2.3, and an age of 13 Gyr. BHB stars and blue stragglers are shown in rectangles. The spectroscopic stars from SDSS DR14 and LAMOST DR6 are shown by red and blue circles respectively.
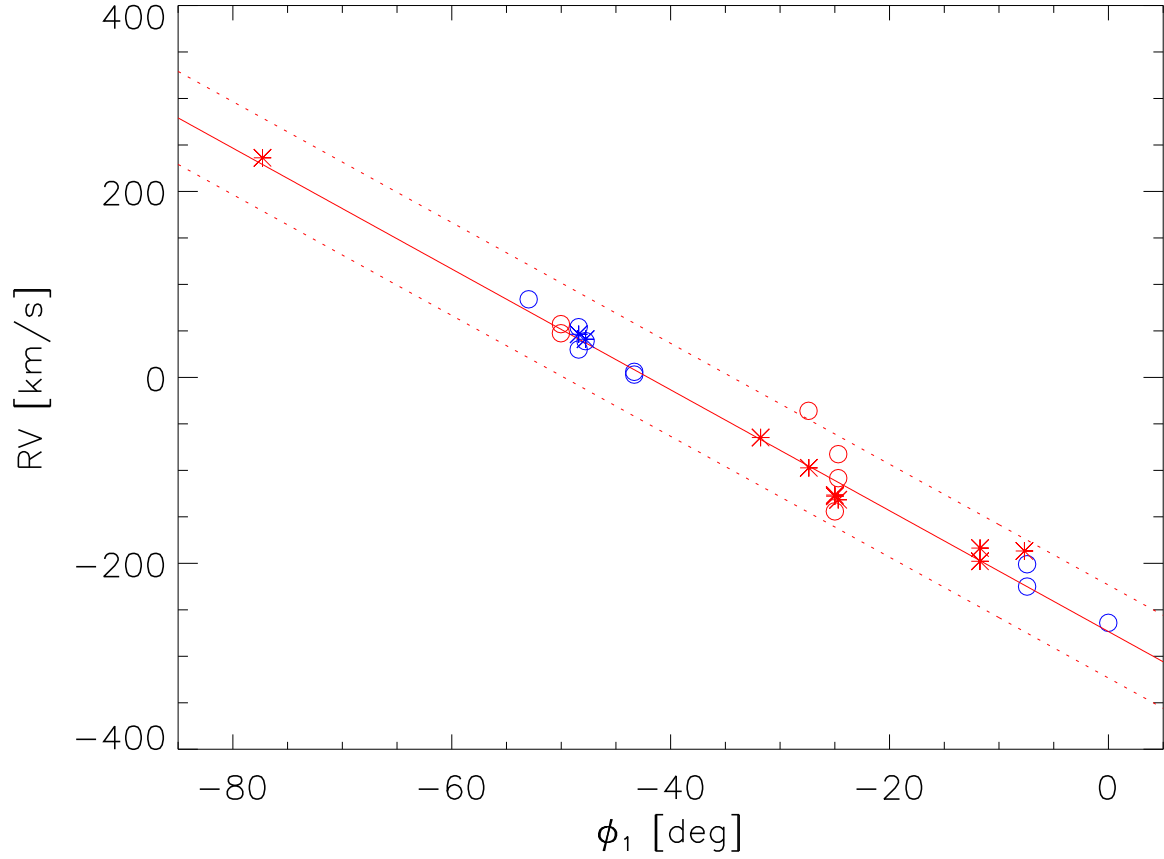
Figure 16. The blue and red symbols are the BHB and BS stars respectively. Circles are the stars from LAMOST DR6, while asterisks are the stars from SDSS DR14. The red circle far from the central line results from low signal-to-noise of LAMOST spectrum. The central red line is $f_4(\phi_1)$ km/s, while the two dotted lines are $f_4(\phi_1) \pm 50$ km/s. One symbol represent one spectrum, so a star may have several symbols.

Table 2. Sky positions

ϕ_1	ϕ_2
[deg]	[deg]
-80	-1.87 ± 0.50
-70	-1.29 ± 0.40
-60	-0.66 ± 0.25
-55	-0.43 ± 0.25
-50	-0.10 ± 0.25
-45	-0.03 ± 0.25
-40	0.13 ± 0.25
-35	0.10 ± 0.20
-30	0.13 ± 0.17
-25	0.06 ± 0.15
-15	-0.11 ± 0.10
-10	-0.23 ± 0.10
-5	-0.71 ± 0.12
0	-1.10 ± 0.15
5	-1.62 ± 0.15

Table 3. SDSS spectra

Spec ID	α	δ	ϕ_1	ϕ_2	$\mu_\alpha cos\delta$	μ_δ	g_0	r_0	[Fe/H]	RV
	[deg]	[deg]	[deg]	[deg]	[mas/yr]	[mas/yr]	[mag]	[mag]	[dex]	[km/s]
1154-53083-0145	126.577155	-0.439391	-82.039695	-1.935876	-1.23	-9.80	19.16	18.96	-2.33 ± 0.28	246.3 ± 20.5
1154-53083-0155	126.645409	-0.340475	-81.919882	-1.946076	-2.66	-10.22	18.16	17.88	-2.14 ± 0.23	259.7 ± 14.4
1154-53083-0633	127.278928	-0.065362	-81.366291	-2.359597	-2.35	-10.32	19.51	19.26	-2.41 ± 0.31	263.9 ± 21.6
1154-53083-0606	127.252030	1.086253	-80.379438	-1.764341	-2.18	-10.54	19.81	19.54	-2.26 ± 0.36	248.1 ± 25.4
3293-54921-0483	130.382898	6.422579	-74.193561	-1.804304	-0.88	-11.44	18.94	18.57	-1.94 ± 0.31	176.4 ± 18.2
5285-55946-0230	130.258665	7.781532	-73.080699	-1.014204	-2.32	-11.60	18.44	18.20	-2.09 ± 0.29	213.6 ± 20.7
... ...	...									

Note: Only a portion of table is shown here for illustration. The whole table contains information of 136 spectra from 116 individual stars are available in the online electronic version. The spectral parameters are calculated by ULySS with ELODIE interpolator. BHB and BS spectra are not given here.

Table 4. LAMOST spectra

Spec ID	α	δ	ϕ_1	ϕ_2	$\mu_\alpha cos\delta$	μ_δ	g_0	r_0	[Fe/H]	RV
	[deg]	[deg]	[deg]	[deg]	[mas/yr]	[mas/yr]	[mag]	[mag]	[dex]	[km/s]
20170101HD093318N282204M0202028	141.661364	26.841665	-51.177836	-0.194631	-4.60	-13.22	16.98	16.55	-1.97 ± 0.11	69.2 ± 5.7
20170226HD092331N251058B0112136	141.661364	26.841665	-51.177836	-0.194631	-4.60	-13.22	16.98	16.55	-2.15 ± 0.06	55.8 ± 3.1
20161126HD091735N272519M0206144	141.568500	26.967834	-51.119222	-0.055559	-4.65	-12.96	18.11	17.76	-2.45 ± 0.09	56.0 ± 6.8
20170101HD093318N282204M0203077	141.779273	28.159696	-50.025682	0.453987	-4.89	-12.97	17.38	17.32	-2.15 ± 0.03	79.3 ± 3.6
20170101HD093318N282204M0215077	142.787822	29.461088	-48.452579	0.453902	-4.38	-13.29	17.47	17.06	-2.16 ± 0.07	39.6 ± 4.4
20131113HD093318N282204B0112045	144.806430	30.124543	-46.905954	-0.602918	-5.11	-13.10	16.60	16.13	-1.80 ± 0.11	31.2 ± 5.1
20170129HD094135N311640B0205233	144.806430	30.124543	-46.905954	-0.602918	-5.11	-13.10	16.60	16.13	-2.02 ± 0.05	41.5 ± 2.5
20111227F559230403032	144.120941	30.947720	-46.574397	0.354304	-4.85	-13.35	17.98	17.75	-2.17 ± 0.25	9.9 ± 13.9
20111220B559160614045	145.582829	31.777470	-45.174505	-0.181384	-5.19	-12.69	14.94	14.56	-1.86 ± 0.08	11.7 ± 4.4
20130413HD094135N311640F0104221	145.582829	31.777470	-45.174505	-0.181384	-5.19	-12.69	14.94	14.56	-1.95 ± 0.04	15.3 ± 2.2
20121120HIP4761705133	145.582829	31.777470	-45.174505	-0.181384	-5.19	-12.69	14.94	14.56	-2.05 ± 0.04	22.2 ± 2.2
20120121F559480311141	145.676545	32.363379	-44.653108	0.097439	-5.17	-12.88	16.07	15.57	-2.29 ± 0.12	-8.4 ± 4.9
20130413HD094135N311640F0115133	145.676545	32.363379	-44.653108	0.097439	-5.17	-12.88	16.07	15.57	-2.28 ± 0.10	11.6 ± 5.4
20170129HD094135N311640B0209118	145.676545	32.363379	-44.653108	0.097439	-5.17	-12.88	16.07	15.57	-2.33 ± 0.04	18.4 ± 1.8
20170317HD093848N300911B0112245	145.676545	32.363379	-44.653108	0.097439	-5.17	-12.88	16.07	15.57	-2.28 ± 0.13	20.2 ± 6.4
20111227F559230412143	146.108792	32.808579	-44.078864	0.064429	-5.03	-12.83	17.40	17.01	-2.24 ± 0.26	-8.7 ± 19.5
20131206HD095000N333605M0105199	146.108792	32.808579	-44.078864	0.064429	-5.03	-12.83	17.40	17.01	-2.26 ± 0.06	8.8 ± 2.9
20170403HIP48512gw0109157	148.804229	35.888640	-40.279970	0.131574	-5.56	-12.60	14.10	13.44	-2.50 ± 0.03	-12.8 ± 1.9
20120122F559490405166	152.583159	39.754518	-35.397703	0.224503	-6.11	-12.40	17.37	16.90	-2.00 ± 0.12	-35.7 ± 6.9
20130306HD102234N423659M0103249	153.787485	42.230398	-32.921557	1.133103	-6.18	-12.08	13.91	13.24	-2.38 ± 0.02	-68.8 ± 1.5
20130306HD102234N423659B0103249	153.787485	42.230398	-32.921557	1.133103	-6.18	-12.08	13.91	13.24	-2.38 ± 0.03	-69.3 ± 2.2
20150423HD102234N423659V0103249	153.787485	42.230398	-32.921557	1.133103	-6.18	-12.08	13.91	13.24	-2.35 ± 0.02	-64.9 ± 1.2
20151231HD104520N453358B0211053	162.052840	47.145408	-25.318253	0.253396	-6.98	-10.66	14.98	14.43	-2.23 ± 0.05	-121.6 ± 2.5
20180112HD105331N491352M0208053	165.199468	48.669257	-22.733558	-0.044503	-7.37	-9.78	17.90	17.52	-2.12 ± 0.08	-152.8 ± 4.7
20171211HD105355N474016B0112011	166.018999	49.153350	-22.009486	-0.031736	-7.26	-9.99	16.48	15.92	-2.00 ± 0.10	-146.1 ± 4.7
20120218F559761207198	175.556867	53.177612	-14.819942	-0.412337	-7.35	-7.73	16.69	16.21	-2.29 ± 0.14	-208.1 ± 10.6
20120103F559300310163	181.925102	55.559525	-10.416717	-0.249590	-7.87	-6.88	16.23	15.71	-2.49 ± 0.08	-210.6 ± 4.9
20170418HD121217N554221B0203180	181.925102	55.559525	-10.416717	-0.249590	-7.87	-6.88	16.23	15.71	-2.27 ± 0.05	-214.9 ± 2.3
20180207HD121650N561653B0110163	181.925102	55.559525	-10.416717	-0.249590	-7.87	-6.88	16.23	15.71	-2.36 ± 0.04	-206.1 ± 2.2
20120124F559510613168	196.468072	57.077875	-2.381764	-1.845128	-6.33	-2.51	17.69	17.23	-2.06 ± 0.21	-271.4 ± 10.3
20170423HD132545N565813M0215017	200.544391	58.011729	-0.033208	-1.465803	-7.73	-3.93	18.00	17.52	-2.29 ± 0.21	-265.1 ± 12.8
20130521HD140517N563114B0116134	209.542501	58.440027	4.715407	-1.725496	-7.49	-2.51	13.73	12.98	-2.31 ± 0.03	-279.0 ± 1.9

Note: BHB and BS spectra are not given here.

Table 5. Four Overdensities of the GD-1 stream

Name	Range	Center in ϕ_2^c	FWHM	FWHM	Area	Areal Density of Dwarfs
	[deg]	[deg]	[deg]	[pc]	[deg^2]	[counts/deg^2]
O1	[-54, -43]	0.039	0.68	91.9	7.51	25.7
O2	[-37, -23]	-0.051	0.35	49.4	4.84	31.9
O3	[-17, -11]	0.147	0.28	44.6	1.68	50.5
O4	[-3, 2]	-0.115	0.58	104.7	2.91	29.4

Table 6. Spectra of BHB and BS stars in LAMOST DR6

Spec ID	α	δ	ϕ_1	ϕ_2	RV	BHB/BS
	[deg]	[deg]	[deg]	[deg]	[km/s]	
20170226HD092331N251058B0103128	140.236539	25.533824	-52.974503	0.147497	84.4 ± 0.5	BHB
20131113HD093318N282204B0115101	143.453181	29.120593	-48.403614	-0.217124	45.9 ± 0.3	BHB
20120121F559480310187	143.453195	29.120636	-48.403572	-0.217109	16.6 ± 0.6	BHB
20111221F559170516061	143.597817	29.802689	-47.771515	0.068473	35.4 ± 0.4	BHB
20121120HIP4761709243	146.897743	33.258213	-43.324801	-0.202088	2.5 ± 0.3	BHB
20170129HD094135N311640B0212185	146.897748	33.258227	-43.324787	-0.202083	-0.7 ± 0.4	BHB
20160312HD124231N565955B0210048	187.384851	56.062763	-7.434435	-1.125792	-226.4 ± 0.4	BHB
20130512HD124231N565955M0110031	187.384947	56.062809	-7.434368	-1.125771	-202.5 ± 0.7	BHB
20130430HD132545N565813F0115016	200.544099	58.092096	-0.016401	-1.387211	-264.7 ± 0.3	BHB
20161126HD091735N272519M0213010	141.779279	28.159708	-50.025669	0.453988	47.5 ± 5.9	BS
20170101HD093318N282204M0203077	141.779279	28.159708	-50.025669	0.453988	57.3 ± 0.9	BS
20120124F559510406187	159.833867	45.728513	-27.402066	0.310294	-36.0 ± 1.3	BS
20130428HD105331N491352M0101031	162.557740	47.251092	-24.996359	0.094510	-144.1 ± 4.3	BS
20150120HD104520N453358M0112057	162.860793	47.482907	-24.688096	0.123543	-82.6 ± 5.0	BS
20111219F559150601070	162.860859	47.482989	-24.688007	0.123572	-108.4 ± 1.7	BS

Table 7. Spectra of BHB and BS stars in SDSS DR14

Spec ID	α	δ	ϕ_1	ϕ_2	[Fe/H]	RV	BHB/BS
	[deg]	[deg]	[deg]	[deg]	[dex]	[km/s]	
2889-54530-0215	143.453190	29.120642	-48.403570	-0.217102	-2.75 ± 0.14	46.4 ± 1.7	BHB
2889-54530-0225	143.597840	29.802695	-47.771499	0.068460	-2.07 ± 0.02	41.0 ± 1.7	BHB
3287-54941-0068	128.645250	3.846764	-77.291130	-1.596769	-2.08 ± 0.15	236.2 ± 7.1	BS
3258-54884-0411	155.918420	42.360810	-31.781306	0.037050	-1.82 ± 0.21	-64.7 ± 6.3	BS
963-52643-0234	160.206670	45.502724	-27.377587	-0.033768	-2.25 ± 0.07	-97.3 ± 3.2	BS
1018-52672-0247	162.557720	47.251092	-24.996369	0.094520	-1.87 ± 0.02	-126.6 ± 2.6	BS
2390-54094-0225	162.557740	47.251092	-24.996359	0.094510	-1.78 ± 0.07	-127.8 ± 3.7	BS
2390-54094-0256	162.860870	47.482966	-24.688018	0.123550	-1.48 ± 0.03	-131.6 ± 3.2	BS
1186-52646-0137	179.937550	54.872774	-11.741092	-0.305673	-1.91 ± 0.15	-197.8 ± 9.7	BS
1315-52791-0004	180.779680	54.017752	-11.731643	-1.290929	-1.95 ± 0.07	-183.6 ± 9.8	BS
1017-52706-0156	186.460310	56.627599	-7.675466	-0.402289	-2.13 ± 0.11	-186.7 ± 9.2	BS

Note: The spectral parameters [Fe/H] and RV are from the database *sppParams* of SDSS DR14.

Table 8. BHB and BS stars of the GD-1 stream

α	δ	ϕ_1	ϕ_2	$\mu_\alpha cos\delta$	μ_δ	g_0	r_0	Spec	BHB/BS
[deg]	[deg]	[deg]	[deg]	[mas/yr]	[mas/yr]	[mag]	[mag]		
140.236596	25.533821	-52.974477	0.147452	-4.132	-13.037	14.890	15.020	L	BHB
143.453198	29.120633	-48.403573	-0.217112	-4.579	-13.167	15.002	15.234	L, S	BHB
143.597827	29.802693	-47.771507	0.068468	-4.809	-13.145	14.859	14.964	L, S	BHB
146.897744	33.258213	-43.324801	-0.202087	-5.180	-12.972	15.166	15.459	L	BHB
178.682379	54.173819	-12.721899	-0.544864	-7.464	-7.264	15.300	15.408		BHB
187.384947	56.062809	-7.434368	-1.125771	-8.011	-6.015	15.519	15.741	L	BHB
200.544099	58.092096	-0.016401	-1.387211	-7.862	-3.893	15.582	15.704	L	BHB
128.645239	3.846764	-77.291135	-1.596759	-2.325	-10.860	17.710	17.711	S	BS
130.054644	4.380349	-76.125169	-2.547143	-0.720	-9.833	16.294	16.336		BS
141.779273	28.159696	-50.025682	0.453987	-4.887	-12.968	17.384	17.319	S	BS
147.022236	34.374419	-42.366788	0.380009	-5.192	-13.180	17.377	17.560		BS
150.524843	37.541016	-38.128641	0.067106	-5.820	-12.536	18.349	18.294		BS
155.918415	42.360808	-31.781310	0.037052	-6.088	-11.742	18.090	18.107	S	BS
158.774596	46.026867	-27.705490	1.045680	-6.544	-11.697	18.286	18.300		BS
159.833866	45.728510	-27.402069	0.310293	-5.701	-10.161	16.840	16.869	L	BS
160.206653	45.502722	-27.377597	-0.033761	-6.978	-10.723	17.487	17.473	S	BS
162.557771	47.251098	-24.996340	0.094501	-7.011	-10.948	16.959	16.919	L, S	BS
162.860856	47.482985	-24.688012	0.123571	-6.854	-10.264	17.170	17.176	L, S	BS
171.965059	52.272828	-17.123996	0.078116	-7.347	-8.635	18.718	18.645		BS
179.937548	54.872781	-11.741089	-0.305666	-7.842	-7.430	18.229	18.184	S	BS
180.779639	54.017737	-11.731671	-1.290930	-8.547	-7.515	18.455	18.416	S	BS
186.460307	56.627602	-7.675466	-0.402284	-8.353	-5.972	17.630	17.738	S	BS
197.039350	57.925555	-1.860090	-1.109740	-8.144	-4.599	18.368	18.312		BS
197.840722	57.840959	-1.469860	-1.300677	-6.826	-2.321	17.706	17.774		BS
199.283127	58.341687	-0.609431	-0.997524	-7.900	-3.862	17.266	17.427		BS
205.070442	58.460079	2.391450	-1.447635	-7.768	-2.961	18.061	18.167		BS
205.717415	59.492334	2.865133	-0.471724	-7.466	-2.065	16.682	16.782		BS
205.887381	59.186247	2.910395	-0.786611	-5.876	-4.208	17.250	17.288		BS

Note: "L" indicates that the object has one or more spectra in LAMOST DR6 in Table 6; "S" indicates that the object has one or more spectra in SDSS DR14 in Table 7.